RSC Advances

ROYAL SOCIETY OF CHEMISTRY

www.rsc.org/advances

Multi-layered Graphene Quantum Dots derived Photodegradation mechanism of Methylene Blue

*Sima Umrao[†], Poornima Sharma[†], Anushka Bansal[£], Ranjna Sinha[¥], Ranjan Kumar Singh[†], Anchal Srivastva[†,] **

[†]Department of Physics, Banaras Hindu University, Varanasi-221005, India.

[£] Department of Metallurgical Engineering, Indian Institute of Technology-B. H. U., Varanasi, 221005, India

[¥]National Bureau of Fish Genetic Resources, Lucknow, India

*** Corresponding author**

Phone: (+091) 542 2307 308, e-mail: anchalbhu@gmail.com (Dr. Anchal Srivastava)

Abstract

The photocatalytic degradation of methylene blue (MB) under visible light in the presence of multi-layered graphene quantum dots (MLGQDs) phtotcatalyst has been investigated in aqueous heterogeneous solution. The photodegradation mechanism following pseudo first order kinetics were examined for the effects of the existing monomer (MB^+)-dimer {$(MB^+)_2$} equilibrium in MB solution. The photocatalytic degradation efficiency of MB^+ achieved 93.3% with a rate constant (k) 0.056 min^{-1} after 60 min irradiation of green light, while less degradation 89.44% with k ~ 0.024 min^{-1} was achieved for $(MB^+)_2$. MB^+ perhaps short-lived species and favoring the photodegradation of MB in comparison to $(MB^+)_2$ species. Similar trend have been found under blue light irradiation. MB^+ species easily pull proton from the functional group of MLGQDs, resulting an intermediate product Luco-methylene blue (LMB). Finally all MB species and intermediate product degrade into the environmental benign product via highly reactive OH radicals. In addition, our ab initio theoretical result reveals that monomer abstract a proton from hydroxyl group of MLGQDs and formation of LMB takes place which is weakly bonded with MLGQDs by hydrogen bond.

Key Words: Multi-layered Graphene quantum dot, Photocatalysis, Methylene Blue, Visible light, DFT

Introduction

In recent years, heterogeneous photocatalysis has emerged as an advanced green technology due to its potential to purify wastewater that is discharged from industries.[1] Heterogeneous photocatalysts offer great potential for generating reactive oxygen species (like OH free radicals) and therefore decompose organic contaminants. Organic contaminants once released into the aquatic ecosystem can generate numerous environmental problems such as depressing light penetration, affect photosynthesis and adversely affecting aquatic biota.[2,3] Unfortunately, deep colored methylene blue (MB) dye discharges widely in wastewater from dyeing, feather, textile, and any other industries and the existence of MB in water can cause virulent irritation on eye, nausea, vomiting and diarrhoea.[2,4,5]

To date, large variety of traditional heterogeneous photocatalyst such as transition metal oxides semiconductors (such as TiO_2) and including their hybrids with noble metals, quantum dots, non-metal doped semiconductors, carbon nanotubes and graphene derivatives have been used for the photodegradation MB in effluents under UV and visible light irradiation[1,5–25] However, in the above studies, none have focused on the degradation mechanism of MB. Need of the day is to find new class of low cost photocatalyst which show high efficiency, high rate constant, enhanced absorption of irradiated light, and more absorption of organic molecule. The photodegradation and mechanism of MB is still not explored fully due to its better stability and its dimer formation in water.[26]

Recently, owing to the high specific surface area of semiconductor quantum dots (zero dimension), numerous efforts have been made to enhance the catalytic performance of these quantum dots.[17,19] High surface-area of photocatalyst is of great significance to increase absorption of organic dye and photodegradation rate because of photocatalytic reaction occurs at the surface of catalyst. Now a days, graphene quantum dots (GQDs) have been receiving much attention as a new class of co-catalysts, [27–29] which could potentially offer desirable reactive oxygen species for enhancing photocatalytic efficiency. Graphene quantum dots (GQDs) are small graphene fragments, where electronic transport is confined

in all three spatial dimensions. It possess unique properties owing to its structural uniformity with graphene along with the quantum confinement, which make them interesting candidates for a whole range of new applications. With their large abundance, the presence of various oxygen functional group, nontoxicity, high mobility, the extraordinarily long lifetimes of exciton charge carriers, and tuneable band gaps motivated us to explore its potential as photocatalyst. To the best of our knowledge, few efforts have been made to electronically combine GQDs as co-catalyst with other photocatalysts.[30–32] But, there is no report in which GQDs used as main catalyst. Keeping the above points in view, we have planned to study the photocatlytic activity of multi-layered graphene quantum dots (MLGQDs) for degradation of MB.

The present study investigates the mechanism of photodegradation of MB by MLGQDs under two different light green and blue. Our study clearly reveals that photodegradation of MB depend on the present its dimer and monomer species in water. It was found that the photocatalytic degradation efficiency of monomer MB in presence of MLGQDs are found to be 93.3 % and 89.4% with k value ~ 0.056, and 0.054 min^{-1} for green and blue light irradiation respectively after 60 min. irradiation. While, a lower degradation efficiency up to 78.8% and 79.5% with low k value ~ 0.024 and 0.026 min^{-1} was achieved for dimer MB under green and blue light irradiation respectively in the same time. Additionally, density functional theory (DFT) has been performed to understand the interaction of MLGQDs with MB and also calculated highest occupied molecular orbital (HOMO) and lowest unoccupied molecular orbital (LUMO) in these charge transfer compound by time dependent- density functional theory (TD-DFT).

Experimental Section

Materials and Preparation of Multi-layered Graphene Quantum Dots

The one-pot rapid and facile hydrothermal method was used for preparation of zero-dimensional (0D) multi-layered grapheme quantum dots (MLGQDs). Only two ingredients: graphene oxide (GO) synthesized by our group[33,34] using Improved Hummers method[35] and distilled water (DW) were used for synthesis of MLGQDs. GO solution in distilled water (1mg/ml) was put for hydrothermal treatment at 200 ^{0}C for 4 hrs. and finally get a yellow color solution of MLGQDs. The resulting yellow colored solution was cooled to room temperature and centrifuged at 8000 rpm for 10 minutes to removing unreacted GO sheets.

Characterization

The morphology of the as synthesized sample was investigated through transmission electron microscopy (TEM) using a FEI – Tecnai-20 electron microscope. The height of the MLGQDs samples was characterized by using atomic force microscope (AFM) (N8 NEOS Senterra) in non-contact mode. Raman spectra were obtained with a micro-Raman setup (HR LabRam inverse system, JobinYvon Horiba), the 532 nm line from a frequency doubled Nd:YAG laser (Coherent Compass) was used as excitation wavelength. Multi-Purpose X-Ray Photoelectron Spectroscopy (XPS) (Sigma Probe, Thermo VG Scientific), and X-ray diffraction (XRD) (diffractometer system-XPERT-PRO) using Cu-$K_{\alpha 1}$ radiation (λ=1.5405980 Å) were used for characterization of the as-synthesized MLGQDs. Fourier transform infrared spectra (FTIR) of the samples were recorded using a Perkin Elmer Spectrum 65, FT-IR spectrometer. Photoluminescence (PL) spectra were measured on a fluorescence spectrophotometer (PerkinElmer) with an excitation wavelength of 300 nm. The EIS measurements were carried out on a PARSTAT 2273 potentiostat/galvanostat (Advanced Measurement Technology Inc., NPL, Delhi) by using three-electrode cells. The dye degradation level was measured using a UV/VIS/NIR Spectrophotometer (JASCO-V-670, with PMT and PbS detectors).

Photocatalytic Activity test

The photocatalysis experiment was carried out in normal glass bottle containing stock solution of MLGQDs-MB. The stock solution of MLGQDs–MB has been prepared by mixing 19.25 ml (1mg/1ml in DW) of MB solution and 1.75 ml (1mg/1ml in DW) of MLGQDs. The mixed solution was stirred for well absorption and used for further measurement. UV-Vis absorption spectroscopy was used to study the degradation of MB. The solution of MLGQDs-MB was irradiated separately by two normal LEDs light of power ~ 1 W mm^2 (central wavelength ca. at 470 and 520 nm) under constant stirring using normal at regular time intervals (10 min). After that, the absorption spectra were taken as well as optical photographs of the solution.

Density Functional Theory (DFT) Calculation

Molecular geometries of Methylene blue (MB), Luco-methylene blue (LMB) and graphene quantum dot (MLGQDs) in gas phase were fully optimized by DFT method having Becke's non local three-parameter exchange and correlation functional along with the Lee-Yang-Parr correctional functional (B3LYP).[36,37] Geometry of the transition state (TS) between MLGQDs and MB was also optimized. Vibrational analysis was performed in order to ensure that each total extremum energy obtained was genuine, i.e. each minimum has all real frequencies and each transition state has only one imaginary frequency. Zero-point energy (ZPE) correction to total energy and thermal energy correction to enthalpy were obtained at the B3LYP/6-311++g(d,p) level of theory in gas phase and these corrections were also considered to be valid for the corresponding single point energy calculations performed at the same level of theory. All the calculations were performed by Gaussian 03 program.[38] For visualization of the optimized structures and vibrational modes Gauss View 4.1[39] program was used.

Results and discussion

Structural and spectroscopic characterization

MLGQDs was synthesized employing hydrothermal treatment on GO solution in water. We anticipate that during sonication process and hydrothermal treatment, cutting of GO takes place due to energy produce under elevated temperature and pressure.[29] The systematic presentation for the hydrothermal cutting of GO into MLGQDs have shown in **Figure S1**. **Figure 1(a)** shows the TEM image of MLGQDs which depicts the ~ 8 nm average size particle of MLGQDs as shown in size distribution curve. The high resolution TEM (HRTEM) image (**Figure 1b**) indicates high crystallinity of the MLGQDs with an interlayer spacing ~0.37 nm. The AFM image measured on silicon substrate (**Figure 1c**) shows topographic image of MLGQDs. The height profile of MLGQDs corresponding to line profile 1 and 2 suggest that the no. of layers varies from two to ten.

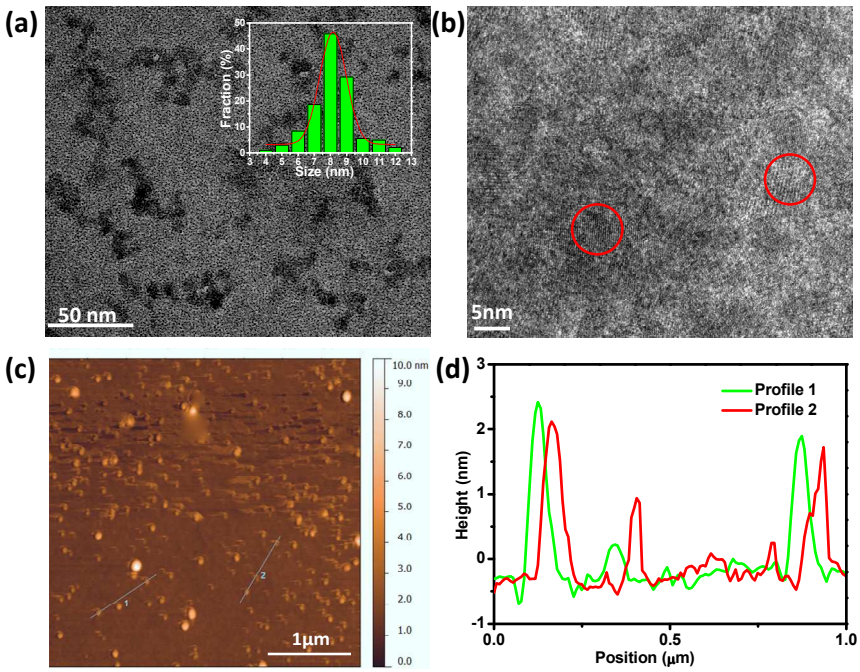

Figure 1. (a) TEM image of MLGQDs; inset size distribution curve well fitted by Gaussian in origin 8.0 software, **(b)** HRTEM image of MLGQDs, **(c)** AFM image of MLGQDs and **(d)** height profile corresponding the line 1 and 2 in AFM image of MLGQDs.

To investigate chemical composition and functional groups of as synthesized MLGQDs, XPS, FT-IR, XRD and Raman measurements have been done. **Figure S2a** shows the core level spectra of C 1s for MLGQDs with its deconvoluted peak positions observed at binding energies of 284.2, 284.8, 286.1, 287.1 and 288.5 eV corresponding to C-C, C=O, C-O, C-OH and COOH bonds, respectively. The FTIR spectrum of MLGQDs (**Figure S2b**) illustrates the presence of C=C stretching (1631cm^{-1}), C=O (1725 cm^{-1}), and C–O (1393 and 1060 cm^{-1}).[28] The relatively broad peak at 3430 cm^{-1} (–OH bending), is due to the adsorbed water content in the surface of MLGQDs. The spectral results described above reflect that MLGQDs have many oxygenated functional groups such as carboxylic, epoxy, alkoxy, hydroxyl and carboxyl groups on their surface, making them hydrophilic nature while the graphite and graphene are hydrophobic in nature.[28,40] The access charges on the surface of MLGQDs prevent their aggregation resulting high surface area for the absorption and the present oxygen functional group support the photo catalytic degradation of MB. Further to confirm the graphitic nature of as synthesized QDs, Raman and XRD measurement have been done. The Raman spectrum of MLGQDs shows two typical peaks at ca. 1349.3 and 1579.3 cm^{-1}, corresponding to the D-band and G-band respectively (**Figure S2c**). The value of I_D/I_G ratio is found ~ 1.22. According to Axel Eckmann et al.,[14] the I_D/I_G ratio varies inversely with crystallite size (L_d) in nano-crystalline graphene [$I_D/I_G \sim 1/(L_d)^2$], where L_d is the length in nm. The calculated crystallite size of as synthesized MLGQDs is ca. 0.90 nm. These results imply that the surfaces of MLGQDs have few structural defects due to presence of various oxygenated groups on the surface.[29,41] In the XRD pattern (**Figure S2d**), the diffraction peak is broad and centered at 24.75 degree corresponding to (0 0 2) reflection plane with interplanar spacing of 0.37 nm. The broad band (0 0 2) peak shows poor crystallization with crystallite size ~ 0.87 nm calculated by Scherrer formula ($L_d = k\lambda/\beta(2\theta).\cos\theta$, where k is dimensionless shape factor equals 0.9, λ is the X-ray wavelength and β is the line broadening at half the maximum intensity (FWHM) after subtracting the instrumental line broadening, in radians), which are nearby the value calculated from Raman result.

The optical properties of MLGQDs are the key to their forthcoming applications in the photcatlysis, energy and biological field.[28,42] Therefore, ultraviolet-visible (UV-vis) absorption, the excitation wavelength dependent photoluminescence (PL) and photoluminescence excitation (PLE) were measured to study optical property of MLGQDs. **Figure 2(a)** shows the UV-vis absorption spectrum of green fluorescent MLGQDs, which exhibits double absorption band edges around 240 and 301 nm and extends to 600 nm without noticeable structures. It shows the absorption peak at 240 nm is ascribed to π-π* transition of aromatic C=C bonds, while a shoulder at 301 nm attributes to n-π* transition of C=O bonds.[43] The optical band gap was calculated using modified Kubelka-Munk function i.e. $[\alpha h\nu]^{1/2}$ ((α is the absorption coefficient, h is Planck's constant, ν is the light frequency) versus hν plot (**Figure 2b**).

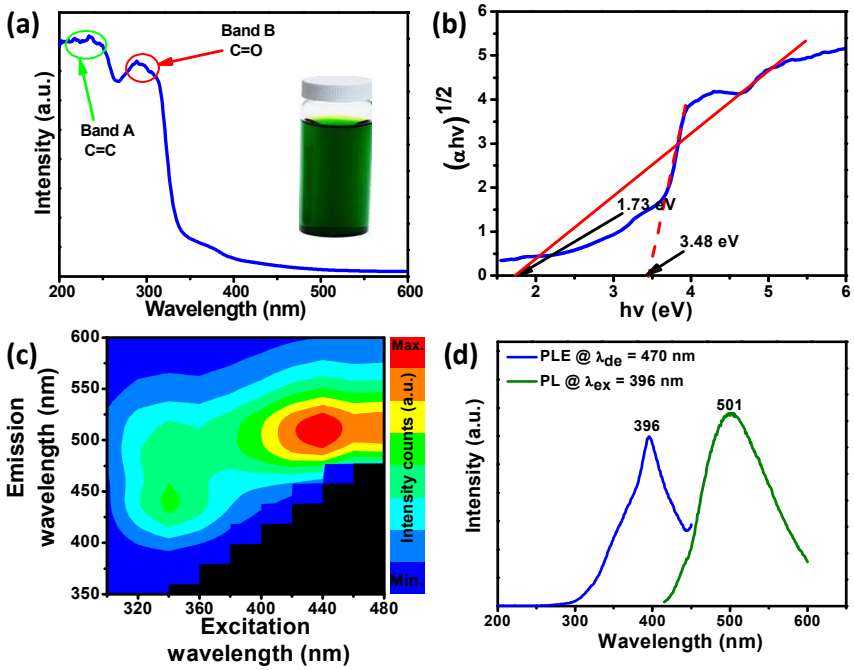

Figure 2. (a) UV-Vis spectra of MLGQDs; inset: optical photographs of the MLGQDs under UV light, **(b)** Tauc plot of transformed Kubelka-Munk function versus the energy of light (hv) for the calculation of band gap (Eg), **(c)** 2D matrices from PL emission spectra of MLGQDs under various excitation wavelength, and **(d)** PLE (the detection wavelength (λ_{de}) of 470 nm) spectra of the MLGQDs and PL (λ_{ex} = 396 nm).

The optical band gap of MLGQDs shows double absorption edges corresponding to a band gap of 3.48 eV and 1.73 eV, which is a virtuous showcase that the MLGQDs will absorb energy in broad range visible to Ultra violet. Because of its novel electronic configurations, MLGQDs shows unique and characteristics spectrum of excitation (absorption) and emission. The PLE spectrum of the MLGQDs was measured using the detection wavelength (λ_{de}) of 470 nm as shown in **Figure 2d** with blue color, showing maximum absorption at 396 nm. Further, PL emission spectrum have been recorded under the maximum absorption (excitation) wavelength 396 nm, which shows the emission maxima at 510 nm corresponding to green fluorescence. There is an overlap between the higher wavelength end of the excitation spectrum and the lower wavelength end of the emission spectrum. When electrons come to the ground state from the excited state, resulting the emission spectrum is shifted to low energy than excitation spectrum due to a loss of vibrational energy.[44,45] This energy shift is ca. 114 nm known as Stokes shift.[45] Additionally, two dimensional (2D) PL intensity map of MLGQDs (**Figure (2c))** was recorded using an excitation wavelength range from 320 to 480 nm with the interval of 20 nm. A broad asymmetric emission consisting two peak ranging from blue (~445 nm) to green (~500 nm) was found with increasing PL intensity corresponding to excitation wavelength (300 to 360 nm). This PL behavior of MLGQDs should be attributed to the multi-photon active process.[44] Moreover, the excitation wavelength range from 380 to 480 nm show a strong symmetric peak at ca. 510 nm which is red shifted and almost invariable in intensity. This green emission can be attributed to quasi-molecular fluorophores,[46] which are formed by the electronic coupling of carboxylic and carbonyl groups for an appropriate chemical reaction. Optical properties of MLGQDs attributed that MLGQDs absorb full range of ultra-violet and visible light, which will support the photocatalysis process for photodegradation of MB.

Photocatalytic degradation of MB in presence of MLGQDs

Illumination of an aqueous solution of MB in presence of MLGQDs results in fast decomposition under visible light irradiation, whereas in the absence of catalyst the degradation is remarkably less (**Figure 3b**.). This study analyzed both the light and time dependent photocatalytic activity of MLGQDs from the photodegradation of toxic colored MB into non-toxic colorless ones under green and blue light irradiation respectively. MLGQDs can degrade MB (blue color) into non-toxic colorless CO_2, H_2O and inorganic anions NO_3^-, SO_4^{2-} etc. under both blue and green light irradiation. First of all, we have investigated an absorption spectra of pure methylene blue solution in water (**Figure 3a**), which reveals that the peak at 614 nm due to the dimer $\{(MB^+)_2\}$ and the peak with enhanced intensity at 664 nm attributed to the monomer species (MB^+). Due to molecular attractive cation-cation interaction, MB^+ molecule exist in dimer $\{(MB^+)_2\}$ species.[26] During photodegradation, the observed change in normalized temporal concentration (C/C_0) of MB^+ and $(MB^+)_2$ is proportional to the normalized maximum absorbance (A/A_0). Here initial concentration (C_0) is regarded as the concentration of MB^+ and $(MB^+)_2$ molecule after adsorption equilibrium.

Figure 3b shows the degradation percentage of MB^+ and $(MB^+)_2$ molecule with reaction rate constant in aqueous solution of MB after irradiation with green and blue light separately. The photodegradation of MB^+ and $(MB^+)_2$ molecule follow pseudo first order reaction well, i.e. $\ln(C/C_0) = -kt$, where C is the final concentration of molecule, C_0 is the initial concentration of molecule, t is the irradiation time, and k is the apparent rate constant. **Figure 3c** depicts the photocatalytic performance of MLGQDs with respect to time. The existence of monomer and dimer species in MB solution in H_2O makes difficult to degrade the dye in proper way because of large unit of dimer species it takes much time for degradation even it presence is in 1.41 times less than monomer. It was found that MB^+ exhibit faster and better photodegradation capability than $(MB^+)_2$ with higher rate constant (**Figure 3b**) under both green and blue irradiation light. After 60 min. irradiation, the photocatalytic degradation efficiency of MB^+ in presence of MLGQDs are found to be 93.3 % and 89.4% with k value ~ 0.056,

and 0.054 min^{-1} for green and blue light irradiation respectively. While a lower degradation efficiency upto 78.8% and 79.5% with low k value ~ 0.024 and 0.026 min^{-1} was achieved for $(MB^{+})_2$ under both irradiation light in the same time. From these results it is clear that in green light irradiation, MLGQDs lead to increased degradation efficiency of dye with high rate constant. The degradation of MB can also be seen in optical photograph of MB solution by changing color from blue to colorless (**Figure S4**).

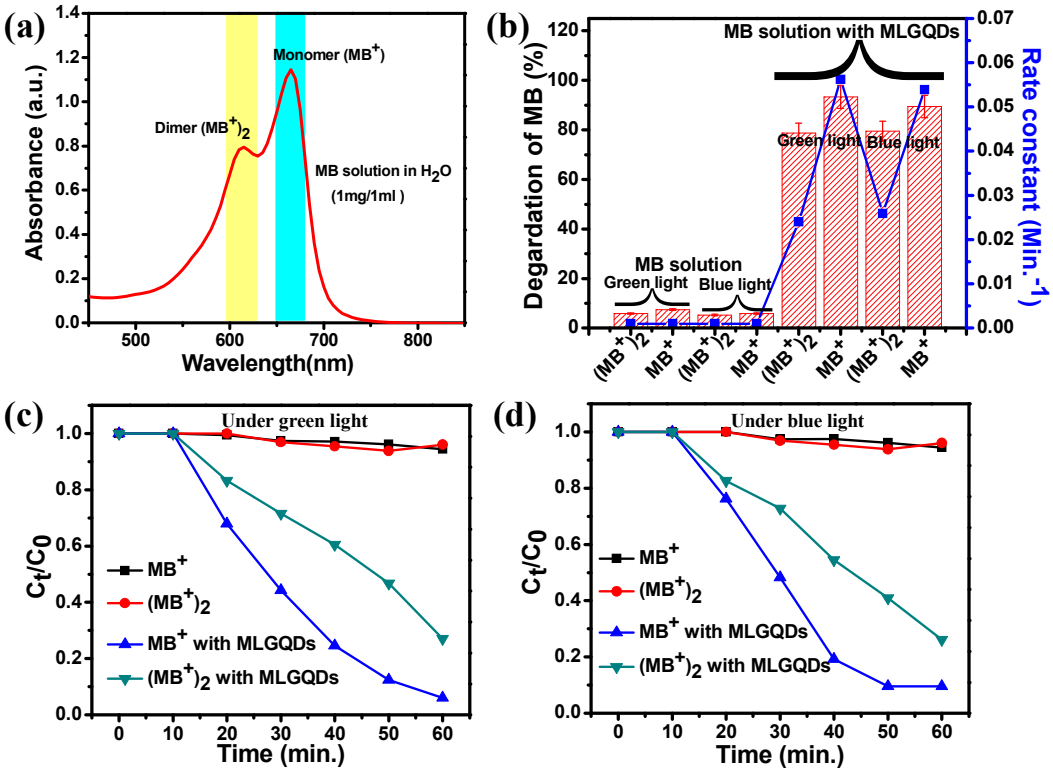

Figure 3. (a) Absorption spectra of MB in H_2O (1mg/1ml), **(b)** the bar plot showing the degradation percentage of monomer and dimer form of MB in solution after 6o minute irradiation with visible light over as-synthesized MLGQDs; **(c)** plot of C_t/C_0 versus irradiation time under Green light and **(d)** plot of C_t/C_0 versus irradiation time under Blue light with same concentration of MB.

After interaction with the MLGQDs in the presence of photo-exicton, the absorption spectra of MB solution carry all the information about the phtotcatalytic activity. 2D imaging of absorption spectra clearly show the spectroscopic changes during the photocatalytic degradation of MB solution under

blue and green irradiation respectively at regular time intervals {**Figure (4 c, d)**}. It clearly shows that the intensity of the MB^+ (absorption at 665 nm) and $(MB^+)_2$ (absorption at 614 nm) decreased steadily. By the perpendicular (horizontal dashed line) spatial coordinate, we obtain a spectroscopic information along the absorption strength along MB^+ and $(MB^+)_2$ species in MB solution.

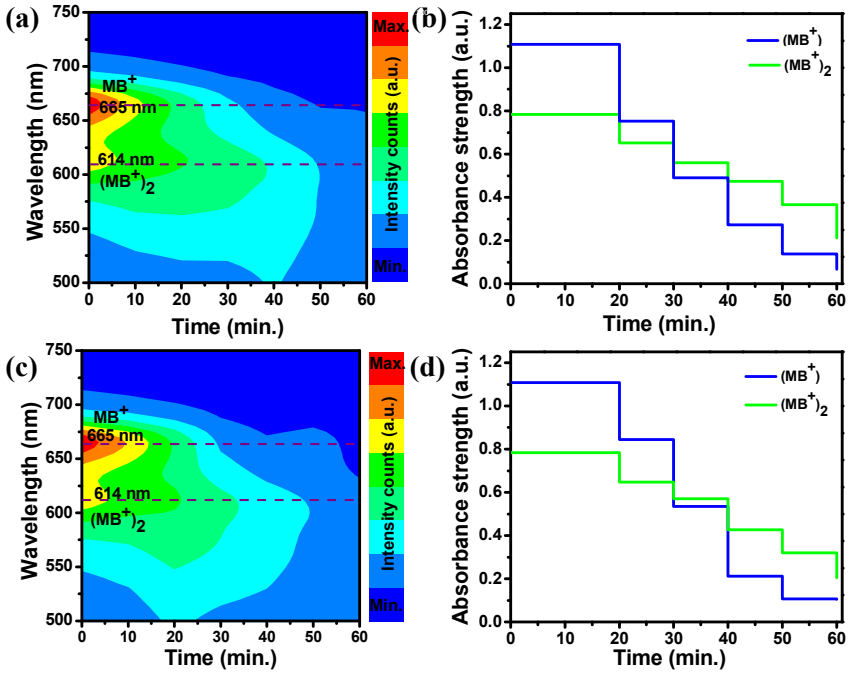

Figure 4. (a), (c) time dependent spectroscopic change on MB when catalyzed by MLGQDs under Green and blue light respectively, and **(b), (d)** a horizontal cross-section at the maximum absorbance change corresponding to time (purple dashed line in (a) and (b)) is shown, depicting the spatial distribution of the absorbance strength with photodegradation of present monomer (MB^+) and dimer ($(MB^+)_2$) in MB cationic dye solution.

The photodegradation of MB^+ remarkably higher than $(MB^+)_2$ even the absorption strength of MB^+ is 1.41 times than $(MB^+)_2$. MB^+ might be short-lived species and favoring the photodegradation of MB in comparison to $(MB^+)_2$. MB^+ may easily convert into Luco-methylene blue (LMB^+) as intermediate product by abstracting proton from functional group of MLGQDs in presence of photoexcited electrons. Photodegradation takes place mainly via highly reactive reagent like OH free radical, which

react with MB^+ and LMB^+ and may degrade into harmless ones CO_2, H_2O and inorganic anions (NO_3^-, SO_4^{2-} etc.). Due to large unit of $(MB^+)_2$ species, it may not easy to degrade into harmless ones. The control experiments, there is no reduction in MB takes place in the conditions, viz., (a) MB in absence of MLGQDs under blue light and (b) MB in absence of MLGQDs under green light irradiation (**Figure S5** in supplementary information). These observations confirmed that the photodegradation of MB occurs in the presence of MLGQDs under visible irradiation. Table 1. summarizes the meticulous comparative analysis of photodegradation efficiencies and rate constants of our MLGQDs with the previously reported TiO_2 based catalyst for MB degradation.

Table 1. Comparative study of photodegradation performance.

Materials	Rate constant value	Photodegradation efficiency	Number of times increase in *k* value over bare TiO_2	Reference
TiO_2	0.0033	36.85	1	[6]
CNT- TiO_2	0.01077	60	3.26	[47]
TiO_2-GR	0.0195	90	5.9	[48]
Pd-fullerene-TiO_2	0.0032	57	0.96	[49]
TiO_2-GO	0.02027	93	6.14	[6]
TiO_2-RGO	0.06209	99	18.81	[6]
MLGQDs	**0.056**	**93.3**	**16.96**	**(present study)**

The plausible mechanism of the photodegradation of MB in presence of MLGQDs under visible light irradiation can be described as follows:

$$MLGQDs + hv \rightarrow MLGQDs\ (e^- + h^+)$$

$$H_2O + h^+ \rightarrow H^+ + OH^\bullet$$

$$H_2O + hv \rightarrow H^+ + OH^-$$

$$OH^- + h^+ \rightarrow OH^\bullet$$

$$MLGQDs + MB^+ \xrightarrow{e^-} MLGQDs\ldots LMB^+ \text{ (colorless)}$$

$$MB^+ \text{ (blue color)} + H+ \xrightarrow{e^-} LMB+ \text{ (colorless)}$$

MB^+ (blue color) + $H^+ \rightarrow LMB^+$ (colorless)

LMB^+ (colorless) + $OH^\bullet \rightarrow CO_2$, H_2O and inorganic anions (NO_3^-, SO_4^{2-} etc.)

$MB^+ + OH^\bullet \rightarrow CO_2$, H_2O and inorganic anions (NO_3^-, SO_4^{2-} etc.)

$(MB^+)_2 + OH^\bullet \rightarrow CO_2$, H_2O and inorganic anions (NO_3^-, SO_4^{2-} etc.)

Since the optical energy band gap of MLGQDs is belonging in a wide range (visible to ultra violet). Therefore, the electron and hole pairs will be generated at the surface of MLGQDs when it excite with an energy higher than the band gap energy of MLGQDs. The defect sites in MLGQDs can act as trapping center for the excited carriers and thereby hinder the recombination process. MB^+ molecules act as a proton acceptor and readily accept a proton from functional group of MLGQDs in the presence of the photoexcited electrons resulting the N–H bond in the MB^+ molecule and thereby changes the color from blue (MB^+) to colorless (LMB^+) as intermediate product. Finally, highly reactive free radicals mineralize all the MB species with particular rate constant.

DFT calculations for the interaction of monomer species of MB with MLGQDs

In order to understand the interaction of MB with MLGQDs, we studied the interaction between MLGQDs and monomer species of MB using DFT. To see the interaction between MLGQDs and MB system, first of all the individual units MLGQDs and MB^+ were optimized. After that, MB–MLGQDs complex was optimized using the optimized individual structures. The optimize structure of MB–MLGQDs complex (**Figure 5a**) reveals that a good interaction occurs *via* a weak hydrogen bonding between MLGQDs and MB system. The hydroxyl functional group (-OH) of MLGQDs plays the role for proton donor and make a hydrogen bond with the nitrogen atom of MB system. The bond length of participated O-H group in hydrogen bonding is enhanced in compared to isolated OH group of MLGQDs from 0.969 Å to 0.976 Å. The bond length of N-C in the central ring of MB is also increased by a considerable amount (from 1.371 Å to 1.395 Å) on interaction.

The dipole moments of MLGQDs and MB are aligned (**Figure 5a**) which is showcase for a strong dipole-dipole interaction. MB abstracts a proton from -OH functional group of MLGQDs during interaction of both and converts into LMB. LMB is bonded with MLGQDs by weak hydrogen bond having typical hydrogen bond length ~ 1.687 Å. The binding energy is obtained after correcting the theoretical results for basis-set superposition error (BSSE). The error due to zero-point harmonic vibrations is also approximately considered. Transition state (TS) calculations were performed in order to understand the reaction mechanism for abstraction of proton from MLGQDs. The formation of LMB through direct proton transfer and corresponding barrier energy at B3LYP/6-311++g(d,p) level of theory is in gas phase. **Figure 5a** shows the structures of reactant complex (RC), transition state (TS), and product (PC) for the gas phase reaction.

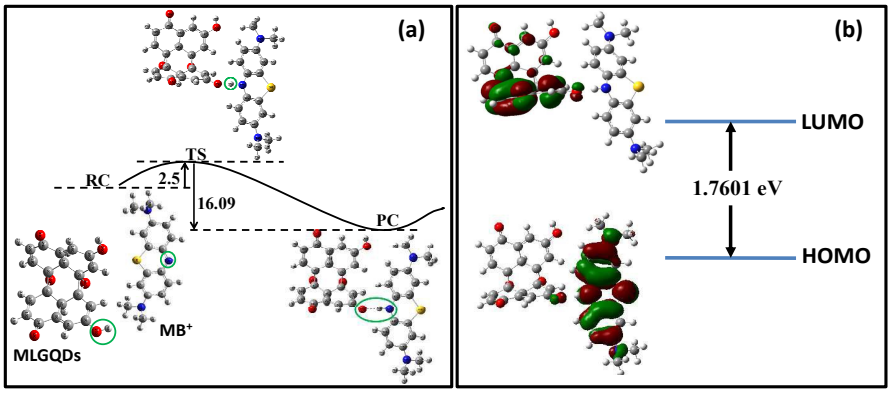

Figure 5. (a) Optimize structure of MLGQDs-MB complex, during optimization MB system abstract a proton from -OH side of MLGQDs and converted to its colorless chemical specie LMB with weak hydrogen bonding to MLGQDs; RC- reactants, TS- transition state and PC- product, **(b)** Chemical structures and distribution of HOMO and LUMO for MLGQDs-MB complex were calculated by TD-DFT level theory.

Activation energies are calculated from the Gibbs free energy differences between the optimized transition state and the optimized reactant complex. The transition state calculations reveal that the moving proton H26 is located between O25 and N19 atoms and C25H26 and N19H26 distances being

1.4086 Å and 1.206 Å respectively. This reaction is predicted to be exothermic as shown by the ZPE-corrected barrier ~ 2.5 kcal/mol and released energies ~ 16.09 kcal/mol at the B3LYP/6-311++g(d,p) level.

The delocalization of HOMO level was designed using DFT calculations in MB-MLGQDs complex system. Consequently, the energy difference between HOMO and LUMO level calculated by TD-DFT. The experimental absorption spectra of MB-MLGQDs complex display common broad bands at around 665 nm with absorption edge from 705 nm due to charge transfer transitions (**Figure S5**). The vertical excitation energies, oscillator strength, composition and tentative nature of transitions obtained at the TD-DFT level of theory (**Figure 5b**). Each absorption line in a TD-DFT spectrum is due to several single excitations. The calculations reveal that the first energy band is dominated by the HOMO / LUMO transition and can be assigned some minimal charge transfer within MLGQDs. However, intensity is relatively weak; therefore this is a local transition (**Figure S6**). The next higher energy transition is correspond to charge transfer from MB to MLGQDs with oscillator strength 0.0425. This transition corresponds to 704 nm excitation wavelength and energy difference between HOMO and LUMO was estimated to be 1.7601 eV along with dipole moment ~ 5.98 eV, which is also evident in our experimental result.

Conclusions

In this study, the photocatalytic activity of MLGQDs was studied by evaluating the mechanism of photodegradation efficiency of methylene blue (MB) in presence of green and blue light emitting diodes (LEDs) as source of visible light. The co-existence of monomer (MB^+) and dimer {$(MB^+)_2$} species in MB solution in H_2O make difficult to degrade the dye as well as to understand degradation mechanism. After 60 min irradiation of green light, 93.3% of photocatalytic degradation of MB^+ with a rate constant (k) 0.056 min^{-1} was achieved, while $(MB^+)_2$ species degrade 89.44% with $k \sim 0.024$ min^{-1}.

Furthermore, we have found the similar trend under blue light. MB^+ easily abstract proton from functional group of MLGQDs, resultant Luco-methylene blue (LMB) as intermediate product and finally photodegradation takes place *via* highly reactive reagent i.e. OH radicals. MB^+ may possibly short-lived species and highly degradable with OH free radicals in comparison to $(MB^+)_2$ species. The photcatalytic reaction are followed by pseudo first-order kinetics. Further, DFT calculations attest the proposed proton transfer mechanism behind the photoreduction of MB and the good interaction with MLGQDs. After interaction of MLGQDs with MB^+, the protons loose from hydroxyl group resulting a short lived intermediate product LMB. In a nutshell, we have successfully investigated the mechanism behind the degradation of MB comprehensively and the encouraging results revealed that monomer species of MB predominated in photodegradation.

***Conflict of Interests*:** The authors declare no competing financial interest.

■ AUTHOR INFORMATION

Corresponding Authors

Address correspondence to anchalbhu@gmail.com

■ Acknowledgements

S.U. is thankful to Mr. Anurag Mishra from Bio-physics lab, BHU, for PL, UV-Vis and FTIR measurements. S.U. is also thankful to Dr. Saurabh Srivastava from NPL, New Delhi, India, for EIS measurement. A.S. acknowledges CAS program sponsored by UGC at Department of Physics, B. H. U and DST, New Delhi, India. S.U. and P.S. express their gratitude for the U.G.C. financial assistances.

■ ASSOCIATED CONTENT

Supporting information DATA: The supporting file includes Schematic for synthesis of MLGQDs, XPS, FTIR, RAMAN, XRD pattern and AC impedance spectra of as synthesized MLGQDs. SI has also included the photographic images of MB-MLGQDs solution as well as time dependent absorbance spectrum of MB alone under Green and Blue light. Optimize structures of MLGQDs, MB, LMB and

ground state HOMO-LUMO level of MLGQDs-MB complex have been also included in supporting information. This material is available free of charge via the Internet at *http://pubs.rsc.org*.

References:

1 S. G. Kumar and L. G. Devi, *J. Phys. Chem. A*, 2011, **115**, 13211–13241.

2 M. Saquib, M. Abu Tariq, M. M. Haque and M. Muneer, *J. Environ. Manage.*, 2008, **88**, 300–306.

3 R. Jain and M. Shrivastava, *J. Hazard. Mater.*, 2008, **152**, 216–20.

4 A.R. Lang (ED.), *Nov. Sci.*, 2009, **New York**, 44–45.

5 E. A. El-Sharkawy, A. Y. Soliman and K. M. Al-Amer, *J. Colloid Interface Sci.*, 2007, **310**, 498–508.

6 S. Umrao, S. Abraham, F. Theil, S. Pandey, V. Ciobota, P. K. Shukla, C. J. Rupp, S. Chakraborty, R. Ahuja, J. Popp, B. Dietzek and A. Srivastava, *RSC Adv.*, 2014, **4**, 59890–59901.

7 A. A. Ismail, D. W. Bahnemann, I. Bannat and M. Wark, *J. Phys. Chem. C*, 2009, **113**, 7429–7435.

8 Y. C. Yang Li , Wen Zhang , Junfeng Niu, *ACS Nano*, 2012, **6**, 5164–5173.

9 D. Wang, Y. Zou, S. Wen and D. Fan, *Appl. Phys. Lett.*, 2009, **95**, 012106–012108.

10 L.-W. Zhang, H.-B. Fu and Y.-F. Zhu, *Adv. Funct. Mater.*, 2008, **18**, 2180–2189.

11 A. Mukherji, R. Marschall, A. Tanksale, C. Sun, S. C. Smith, G. Q. Lu and L. Wang, *Adv. Funct. Mater.*, 2011, **21**, 126–132.

12 S. Al-qaradawi and S. R. Salman, *J. Photochem. Photobiol. A Chem.*, 2002, **148**, 161–168.

13 K. Krishnamoorthy, R. Mohan and S.-J. Kim, *Appl. Phys. Lett.*, 2011, **98**, 244101.

14 N. Zhou, L. Polavarapu, N. Gao, Y. Pan, P. Yuan, Q. Wang and Q.-H. Xu, *Nanoscale*, 2013, **5**, 4236–41.

15 N. Shi, X. Li, T. Fan, H. Zhou, J. Ding, D. Zhang and H. Zhu, *Energy Environ. Sci.*, 2011, **4**, 172.

16 H. Wang, L. Thia, N. Li, X. Ge, Z. Liu and X. Wang, *"Applied Catal. B, Environ.*, 2015, **166-167**, 25–31.

17 X. Shi, X. Xia, G. Cui, N. Deng and Y. Zhao, *"Applied Catal. B, Environ.*, 2015, **163**, 123–128.

18 R. Saada, S. Kellici, T. Heil, D. Morgan and B. Saha, *"Applied Catal. B, Environ.*, 2015, **168-169**, 353–362.

19 J. Hou, C. Yang, Z. Wang, S. Jiao and H. Zhu, *"Applied Catal. B, Environ.*, 2013, **129**, 333–341.

20 J. Podporska-carroll, E. Panaitescu, B. Quilty, L. Wang, L. Menon and S. C. Pillai, *"Applied Catal. B, Environ.*, 2015, **176**, 70–75.

21 K. Tsai and Y. Hsu, *"Applied Catal. B, Environ.*, 2015, **164**, 271–278.

22 C. Cui, Y. Wang, D. Liang, W. Cui, H. Hu, B. Lu, S. Xu, X. Li, C. Wang and Y. Yang, *"Applied Catal. B, Environ.*, 2014, **158-159**, 150–160.

23 M. Seredych and T. J. Bandosz, *"Applied Catal. B, Environ.*, 2014, **147**, 842–850.

24 C. P. Athanasekou, S. Morales-torres, V. Likodimos, G. Em, L. M. Pastrana-martinez, P. Falaras, D. D. Dionysiou, J. L. Faria, J. L. Figueiredo and A. M. T. Silva, *"Applied Catal. B, Environ.*, 2014, **158-159**, 361–372.

25 Y. Li, J. Qu, F. Gao, S. Lv, L. Shi and C. He, *"Applied Catal. B, Environ.*, 2015, **162**, 268–274.

26 J. R. S. Wynetta Spencer, *J. Phys. Chem.*, 1979, **83**, 1573–1576.

27 L. Tang, R. Ji, X. Li, K. S. Teng and S. P. Lau, *Part. Part. Syst. Charact.*, 2013, **30**, 523–531.

28 S. Umrao, M. Jang, J. Oh, G. Kim, S. Sahoo, Y. Cho, A. Srivastva and I. Oh, *Carbon N. Y.*, 2014, **81**, 514–524.

29 D. Pan, J. Zhang, Z. Li and M. Wu, *Adv. Mater.*, 2010, **22**, 734–8.

30 S. Zhuo, M. Shao and S.-T. Lee, *ACS Nano*, 2012, **6**, 1059–64.

31 T.-F. Yeh, C.-Y. Teng, S.-J. Chen and H. Teng, *Adv. Mater.*, 2014, **26**, 3297–303.

32 D. K. L. Chan, P. L. Cheung and J. C. Yu, *Beilstein J. Nanotechnol.*, 2014, **5**, 689–95.

33 V. Kumar, S. Srivastava, S. Umrao, R. Kumar and G. Nath, *RSC Adv.*, 2014, **4**, 2267–2273.

34 S. Srivastava, M. A. Ali, S. Umrao, U. K. Parashar, A. Srivastava, G. Sumana, B. D. Malhotra, S. S. Pandey and S. Hayase, *Appl. Biochem. Biotechnol.*, 2014, **174**, 960–70.

35 D. C. Marcano, D. V Kosynkin, J. M. Berlin, A. Sinitskii, Z. Sun, A. Slesarev, L. B. Alemany, W. Lu and J. M. Tour, *ACS Nano*, 2010, **4**, 4806–4814.

36 A. D. Becke, *J. Chem. Phys.*, 1993, **98**, 5648–5652.

37 R. G. P. Chengteh lee, Weitao Yang, *Phys. Rev. B*, 1988, **37**, 785–789.

38 J. A. P. 3. M.J. Frisch, G.W. Trucks, H.B. Schlegel, G.E. Scuseria, M.A. Robb, J.R. Cheeseman, V.G. Zakrzewski, J.A. Montgomery Jr., R.E. Stratmann, J.C. Burant, S.J. Dapprich, M. Millam, A.D. Daniels, K.N. Kudin, M.C. Strain, O. Farkas, J. Tomasi, V. Barone, M. C, *Pittsburgh PA*, 2003.

39 R. G. R. Dennington II, T. Keith, J. Millam, K. Eppinnett, W.L. Hovell, *Gauss Veiw 4.1, Semichem, Inc., Shawnee Mission.*, 2003, **KS,**.

40 V. Kumar, V. Singh, S. Umrao, V. Parashar, S. Abraham, A. K. Singh, G. Nath, P. S. Saxena and A. Srivastava, *RSC Adv.*, 2014, **4**, 21101–21107.

41 J. Peng, W. Gao, B. K. Gupta, Z. Liu, R. Romero-Aburto, L. Ge, L. Song, L. B. Alemany, X. Zhan, G. Gao, S. A. Vithayathil, B. A. Kaipparettu, A. a Marti, T. Hayashi, J.-J. Zhu and P. M. Ajayan, *Nano Lett.*, 2012, **12**, 844–9.

42 X. Yan, X. Cui, B. Li and L. Li, *Nano Lett.*, 2010, **10**, 1869–73.

43 L. Zhang, X. Li, Y. Huang, Y. Ma, X. Wan and Y. Chen, *Carbon N. Y.*, 2010, **48**, 2367–2371.

44 S. Wu, N. Duan, X. Ma, Y. Xia, H. Wang, Z. Wang and Q. Zhang, *Anal. Chem.*, 2012, **84**, 6263–70.

45 G. G. Guilbault, *Second Ed.*, 1990, **Marcel Dek**, 0–8247– 8350–6.

46 C. Galande, A. D. Mohite, A. V Naumov, W. Gao, L. Ci, A. Ajayan, H. Gao, A. Srivastava, R. B. Weisman and P. M. Ajayan, *Sci. Rep.*, 2011, **1**, 1–4.

47. J. Yu, T. Ma and S. Liu, *Phys. Chem. Chem. Phys.*, 2011, **13**, 3491–3501.

48. N. Yang, Y. Liu, H. Wen, Z. Tang, H. Zhao, Y. Li and D. Wang, *ACS Nano*, 2013, **7**, 1504–1512.

49. Z.-D. Meng, F.-J. Zhang, L. Zhu, C.-Y. Park, T. Ghosh, J.-G. Choi and W.-C. Oh, *Mater. Sci. Eng. C*, 2012, **32**, 2175–2182.

Graphical Abstract

Efficient visible light photodegradation of Methylene blue using multi-layered graphene quantum dots (MLGQDs) has been studied with clear mechanism.